Electronic Supplementary Material (ESI) for Polymer Chemistry.
This journal is © The Royal Society of Chemistry 2018

Supporting Information

The Anionic Ring Opening Polymerization of *N*-(Methanesulfonyl)azetidine

Louis Reisman, Elizabeth A. Rowe, Qiaoli Liang and Paul A. Rupar*
Department of Chemistry, The University of Alabama, Tuscaloosa, Alabama 35487-0336, United States

TABLE OF CONTENTS

Kinetics ……S1

Degradation ……S4

NMR Spectra ……...S5

MALDI-TOF MS Spectra ……...S22

SEC ……..S26

DSC Analysis ……..S26

TGA Analysis ……..S27

References ……...S27

Kinetics

All propagation rates were determined from the linear first order kinetic plots, following equations 1 and 2. Equation 1 shows the reduction of monomer concentration, [M], over time. We assume that the number of active chain ends (P^-) remains constant during the polymerization, therefore, [I] (initiator) = [P^-]. Integration of this equation yields equation 2. Plotting the natural logarithm of monomer consumption with respect to time yields a linear trend, where the slope is (k_{app}). The propagation rate (k_p) is determined by dividing k_{app} by the initial initiator concentration, $[I]_0$. First order kinetics, with respect to monomer, are required for this simplification of equation 2, and has been reported for similar systems, i.e., aziridines.[1-8]

$$\frac{-d[M]}{dt} = k_p[P^-][M] = k_p[I][M] \quad (1)$$

$$ln\frac{[M]_0}{[M]_t} = k_{app}t = k_p[I]_0 t \quad (2)$$

The propagation rate constants, k_p, were determined using the monomer and polymer signals for the polymerizations until a conversion of ≥40% was achieved. An additional point taken at ~90% conversion shows that the rate of polymerization does decrease slightly over time (Figure S1 and S2) for higher [M]:[I] ratios. We hypothesize this is due to an increase in viscosity, which is apparent during these polymerizations.

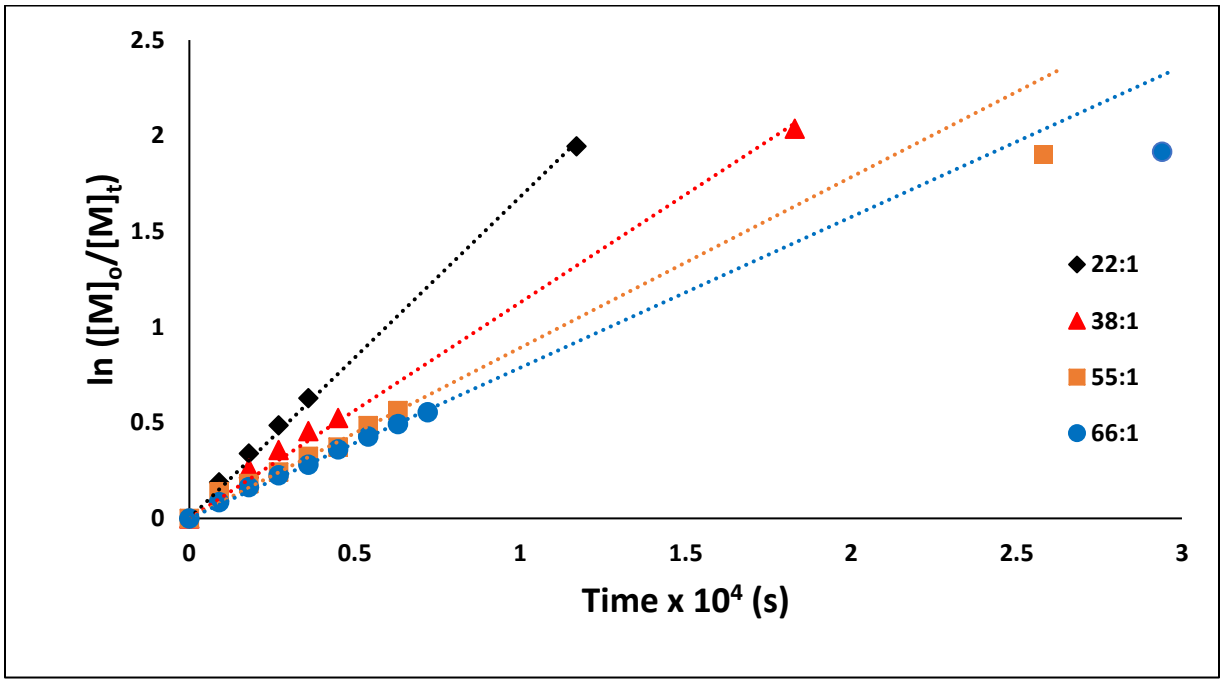

Figure S1. Plot of ln([M_0]/[M_t]) vs time for **MsAzet** polymerization initiated by ^{n}BuN(K)Ms with [M]:[I] ratios ranging from 22:1- 66:1 at 160 °C.

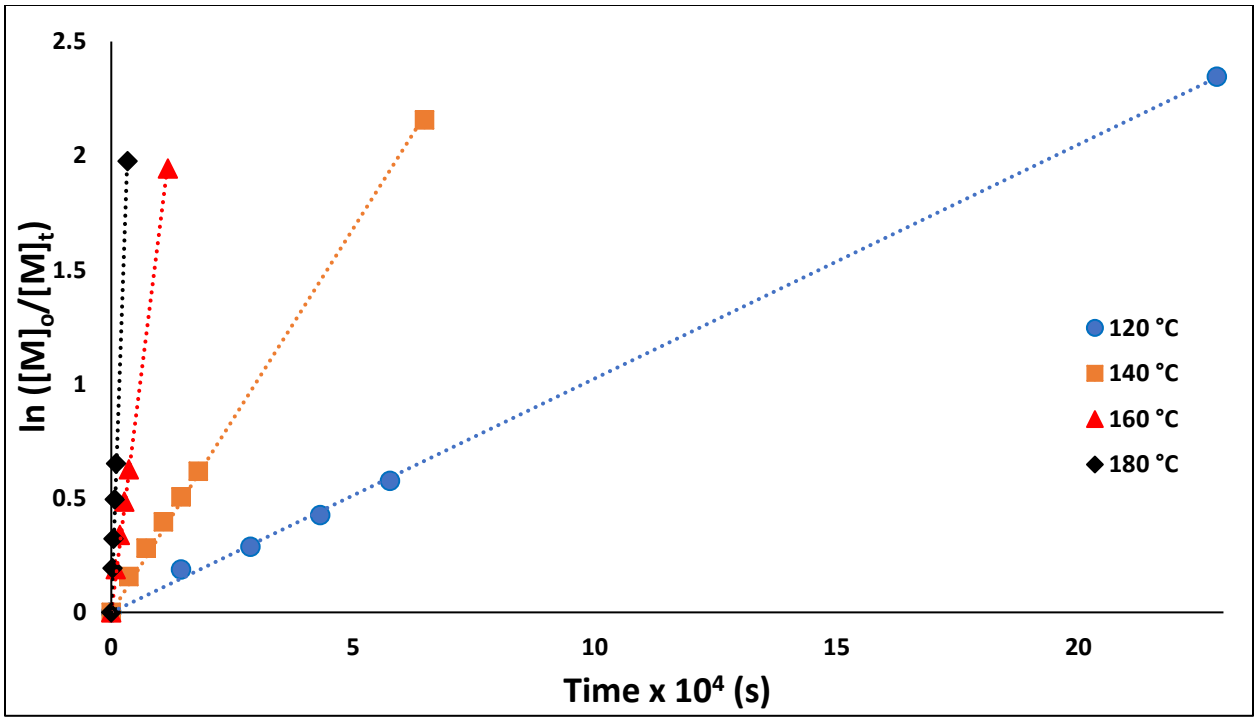

Figure S2. Plots of ln([M_0]/[M_t]) vs time for **MsAzet. MsAzet** polymerization initiated by ^{n}BuN(K)Ms at [M]:[I] ratio of 22:1 and temperatures from 120-180 °C.

Observed Degradation of BnN(K)Ms

Polymerizations of **MsAzet** were initially attempted using BnN(K)Ms as an anionic initiator, as it is widely used in *N*-sulfonylaziridine polymerizations.[1-8] However, the BnNMs end groups of p(MsAzet) were observed to degrade at elevated temperatures. ^{1}H NMR spectroscopy showed that signals attributable to BnNMs decreased in intensity and new aromatic signals appeared (Fig. S3). Due to this complication, ^{n}BuN(K)Ms was used throughout the rest of the study and does not appear to degrade.

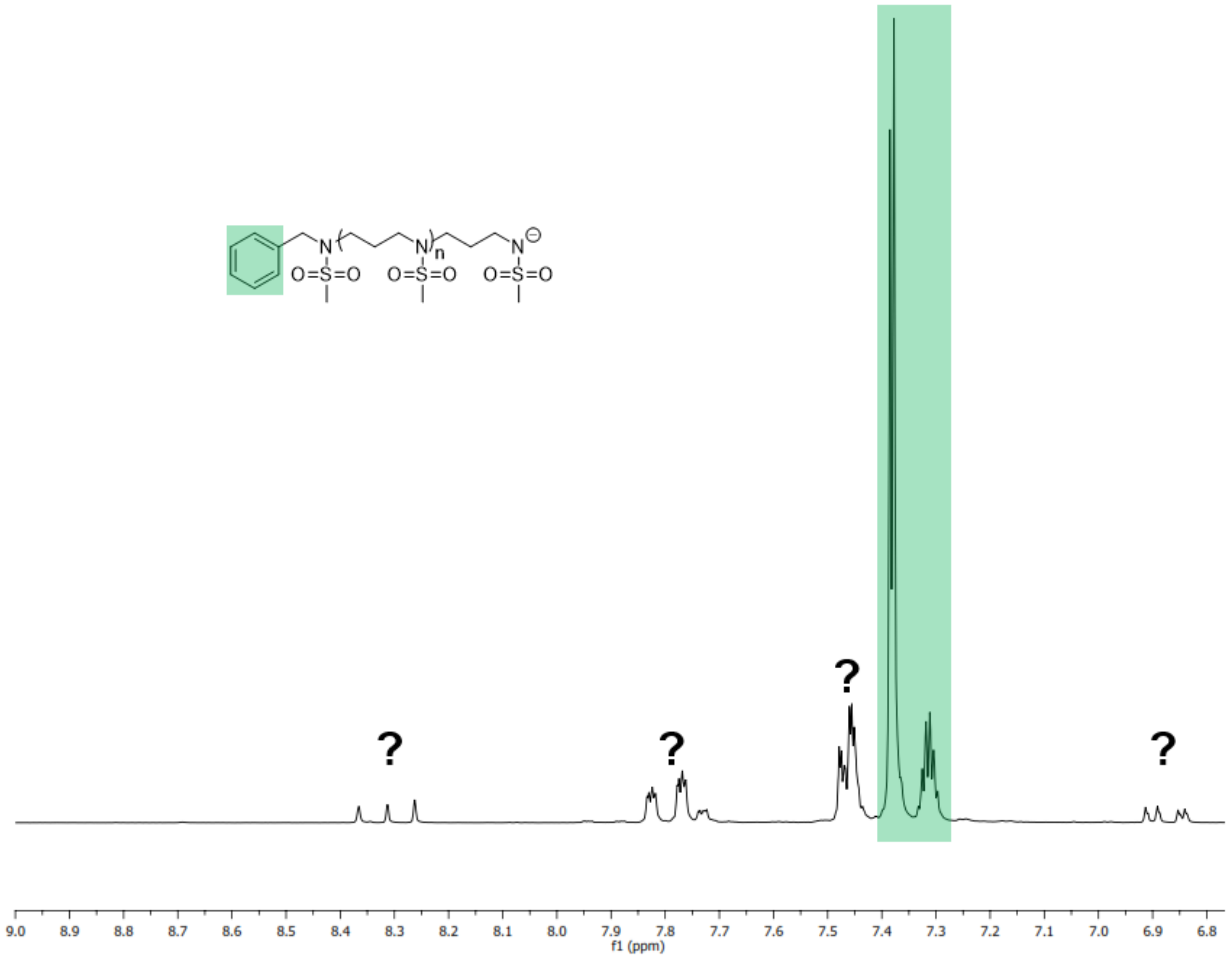

Figure S3. ^{1}H NMR ($DMSO_{d6}$) spectrum displaying the aromatic region of BnNMs initiated living polymerization in anhydrous $DMSO_{d6}$. **?** denotes an unknown signal formed by degradation of the BnNMs endgroups.

NMR Spectra

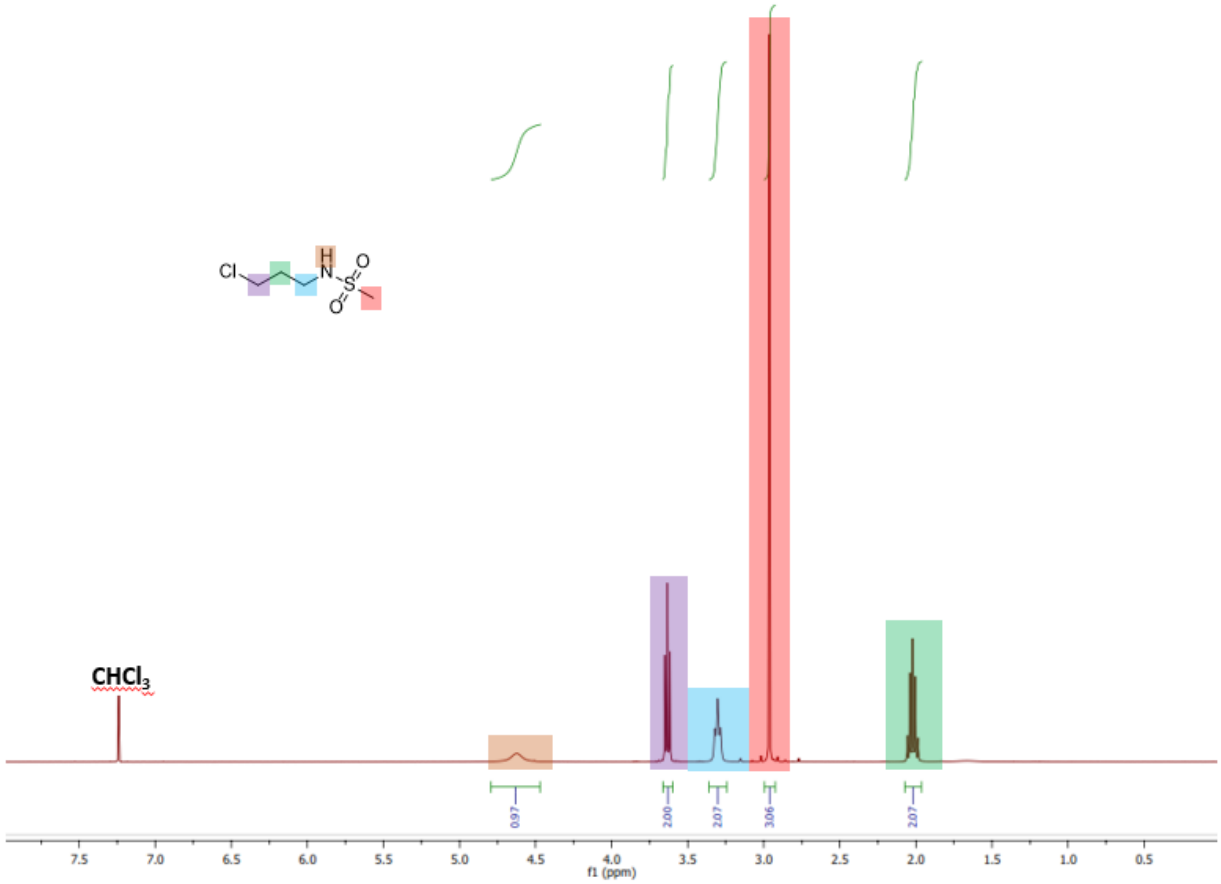

Figure S4. ^{1}H NMR spectrum of *N*-(3-chloropropyl)methanesulfonamide in $CDCl_3$.

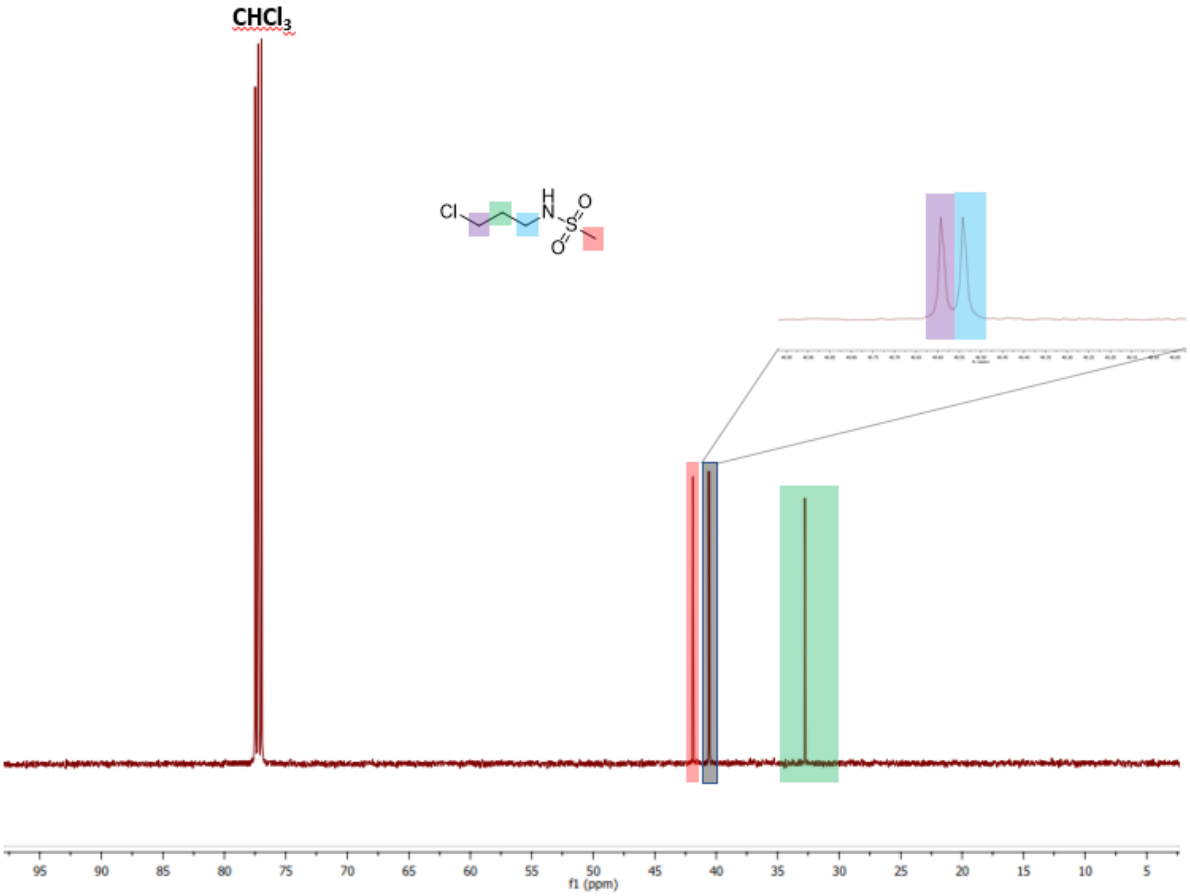

Figure S5. ^{13}C NMR spectrum of *N*-(3-chloropropyl)methanesulfonamide in $CDCl_3$.

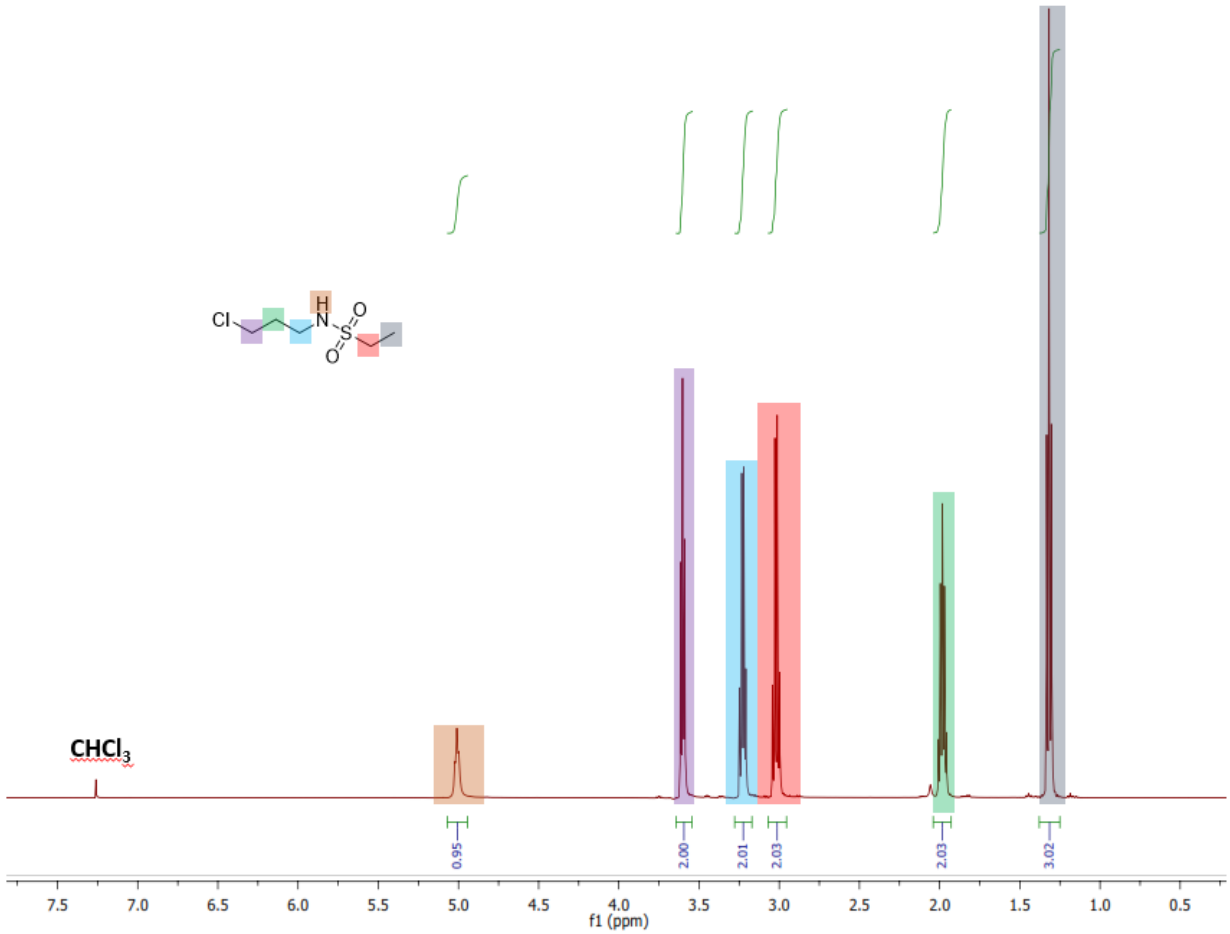

Figure S6. ^{1}H NMR spectrum of *N*-(3-chloropropyl)ethanesulfonamide in $CDCl_3$.

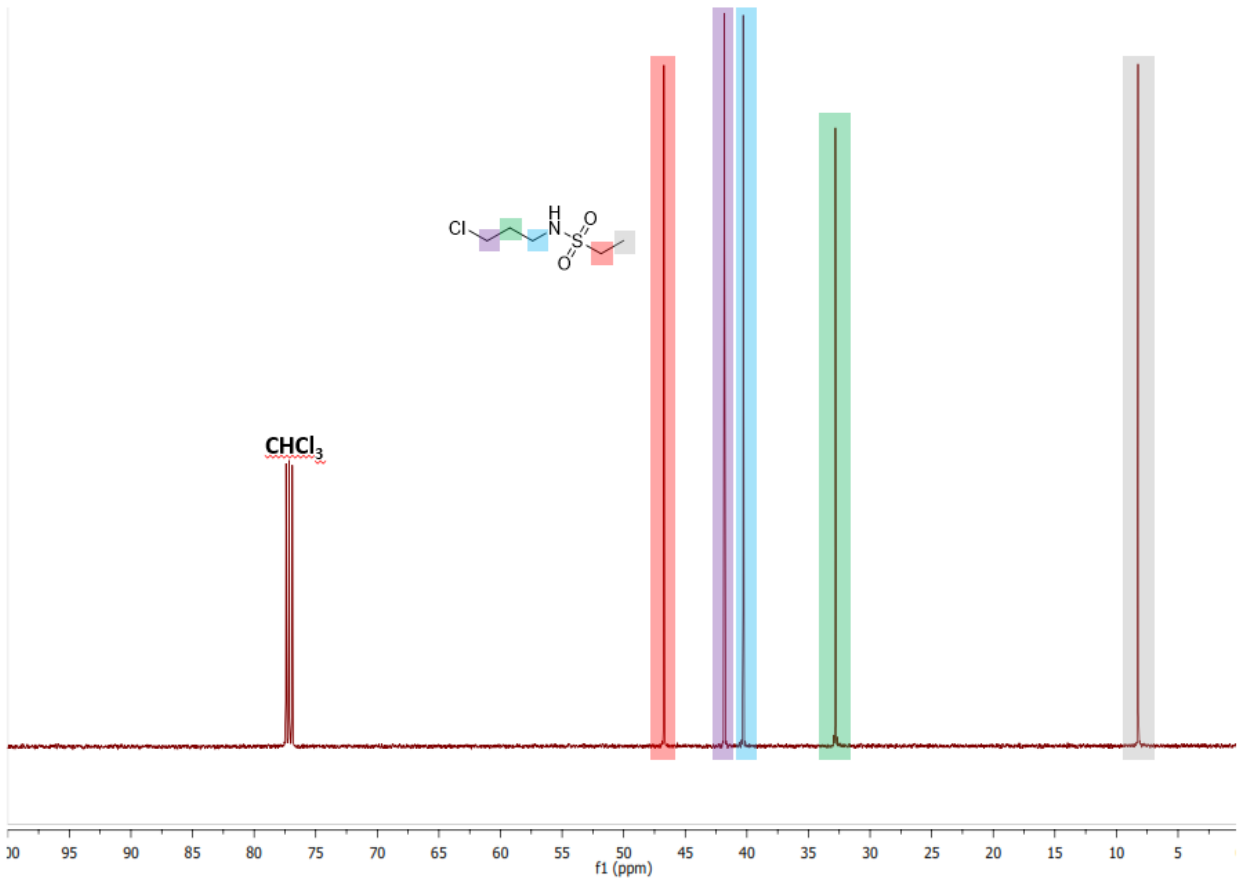

Figure S7. ^{13}C NMR spectrum of *N*-(3-chloropropyl)ethanesulfonamide in $CDCl_3$.

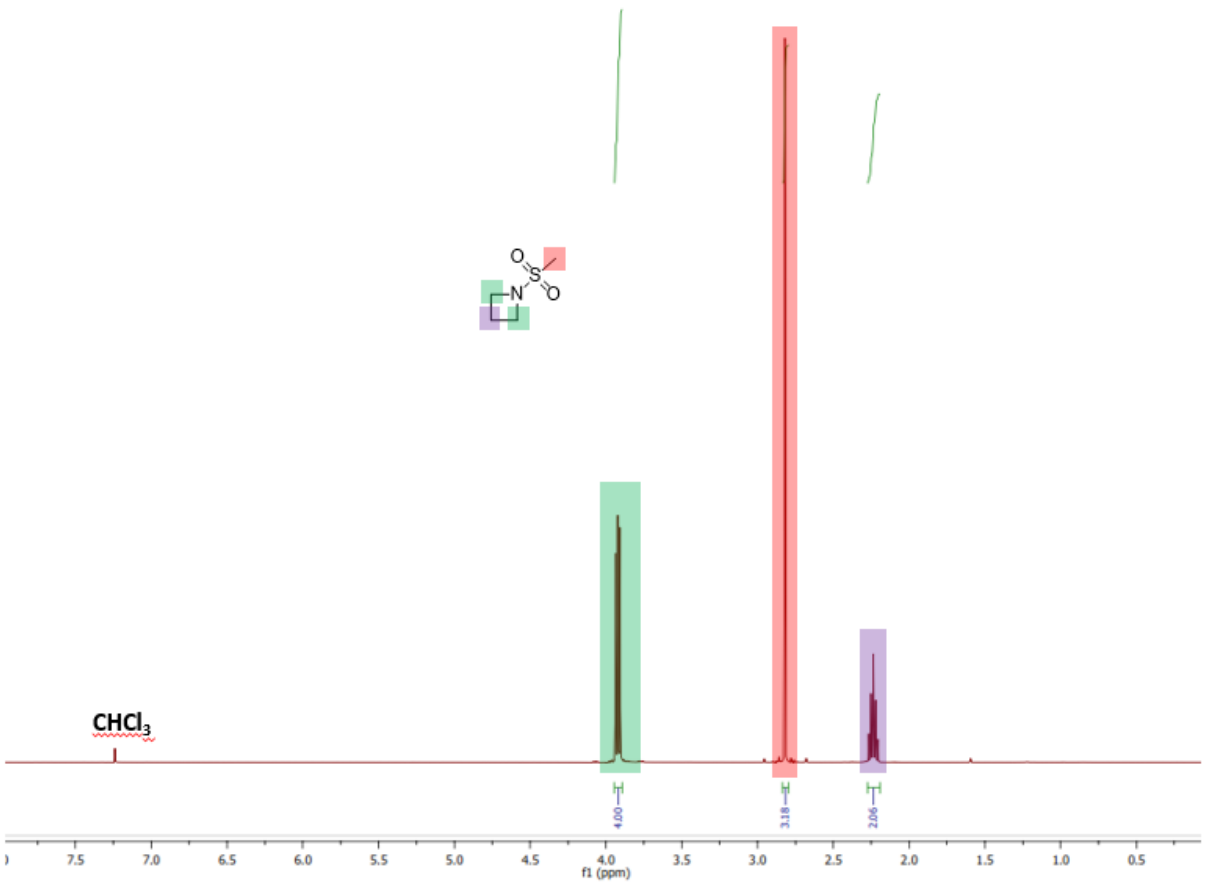

Figure S8. ^{1}H NMR spectrum of **MsAzet** in $CDCl_3$.

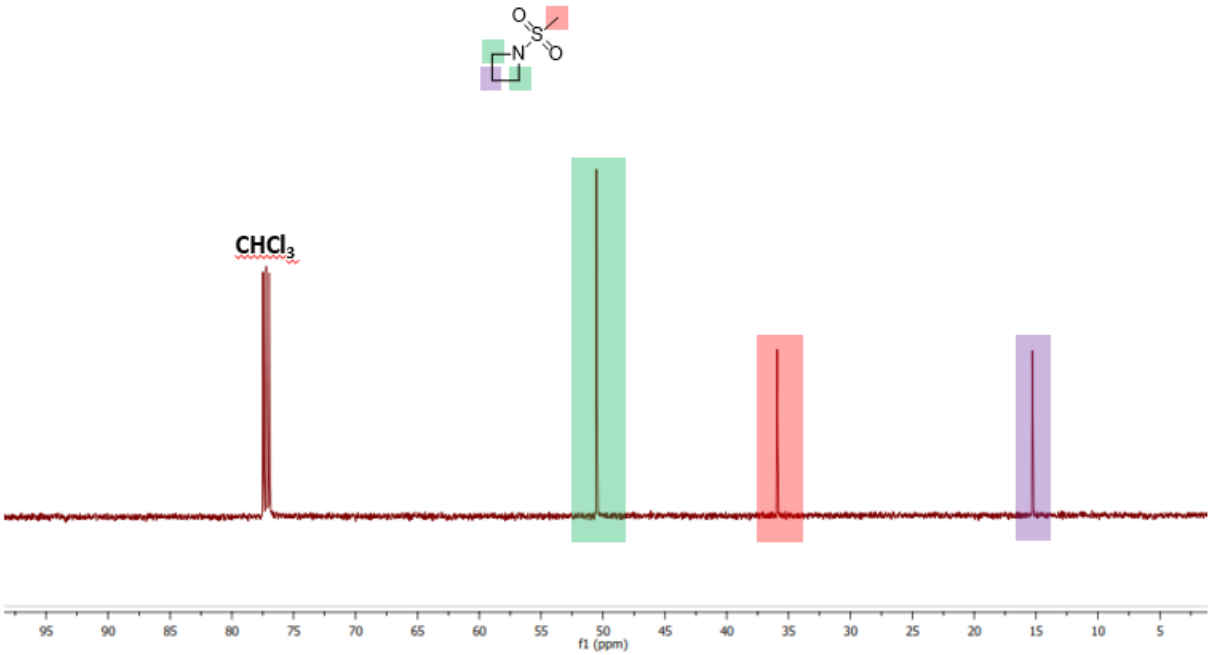

Figure S9. ^{13}C NMR spectrum of **MsAzet** in $CDCl_3$.

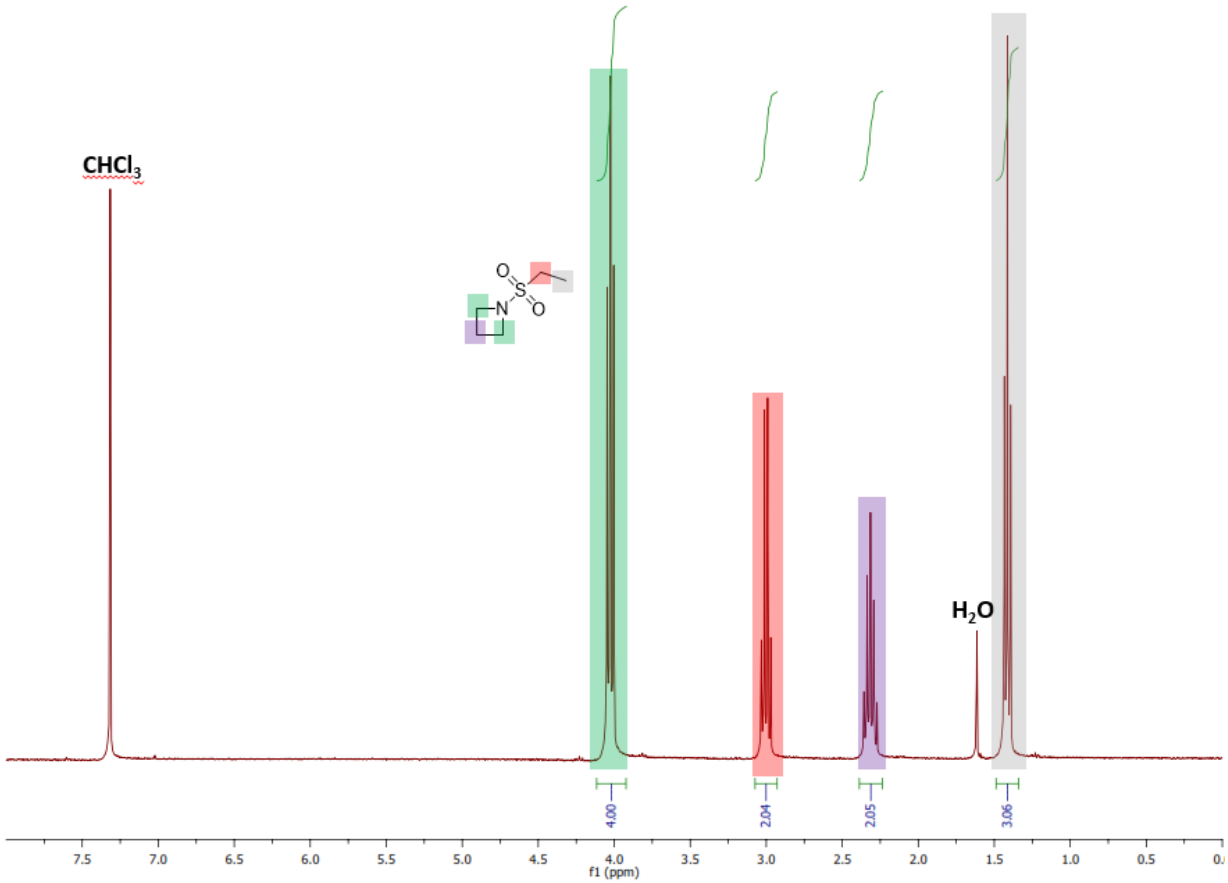

Figure S10. ^{1}H NMR spectrum of **EsAzet** in $CDCl_3$.

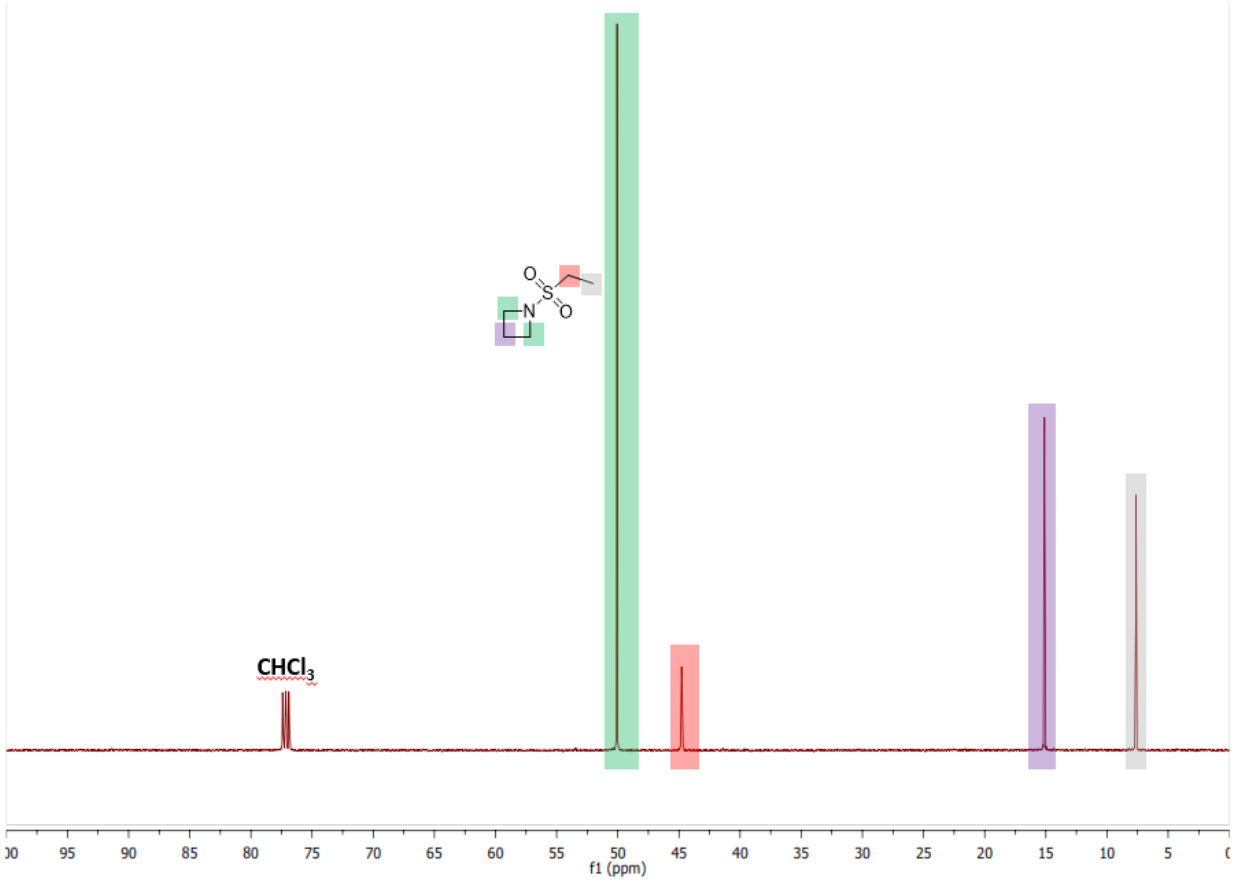

Figure S11. ^{13}C NMR spectrum of **EsAzet** in $CDCl_3$.

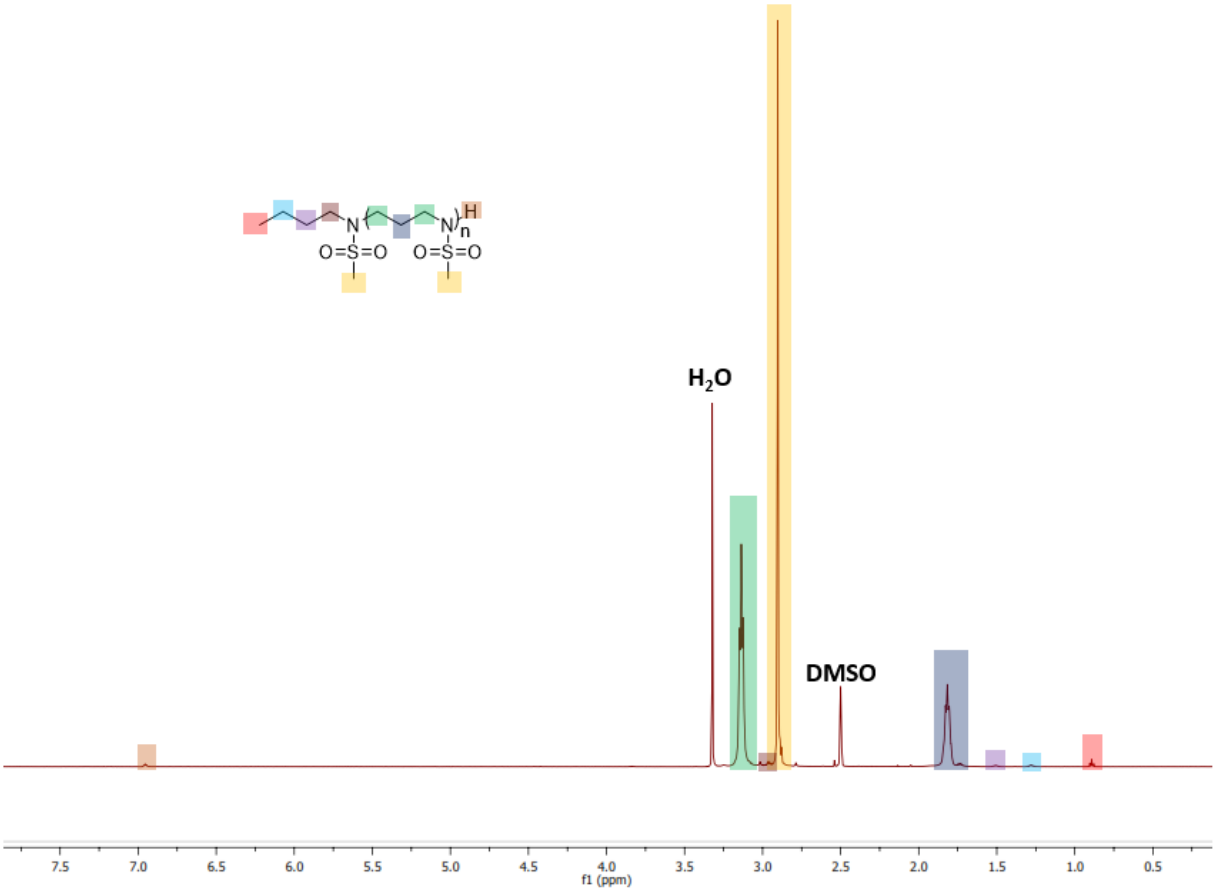

Figure S12. ^{1}H NMR spectrum of non-deuterated p(MsAzet) in $DMSO_{d6}$. This polymer was synthesized in $DMSO_{h6}$.

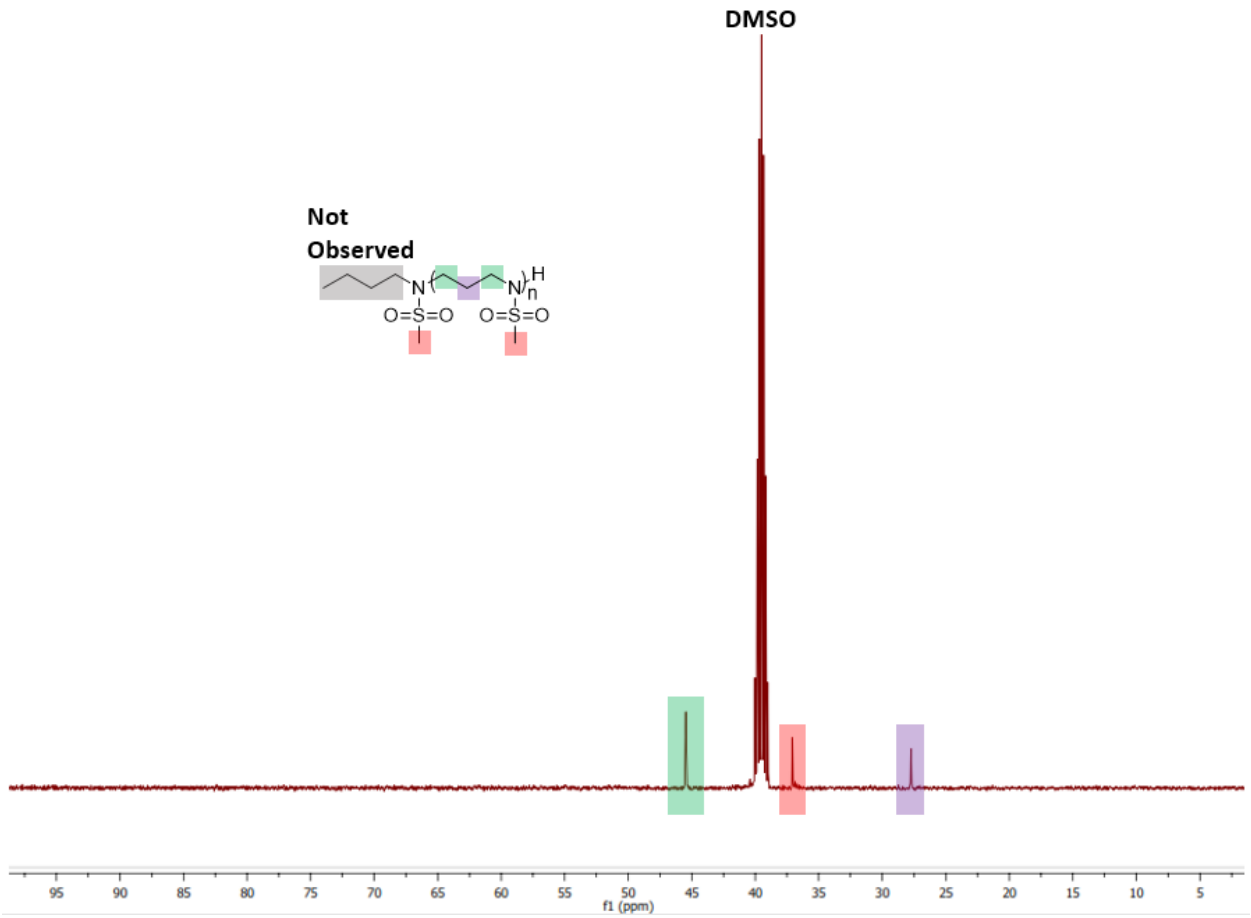

Figure S13. ^{13}C NMR spectrum of non-deuterated p(MsAzet) in $DMSO_{d6}$. This polymer was synthesized in $DMSO_{h6}$.

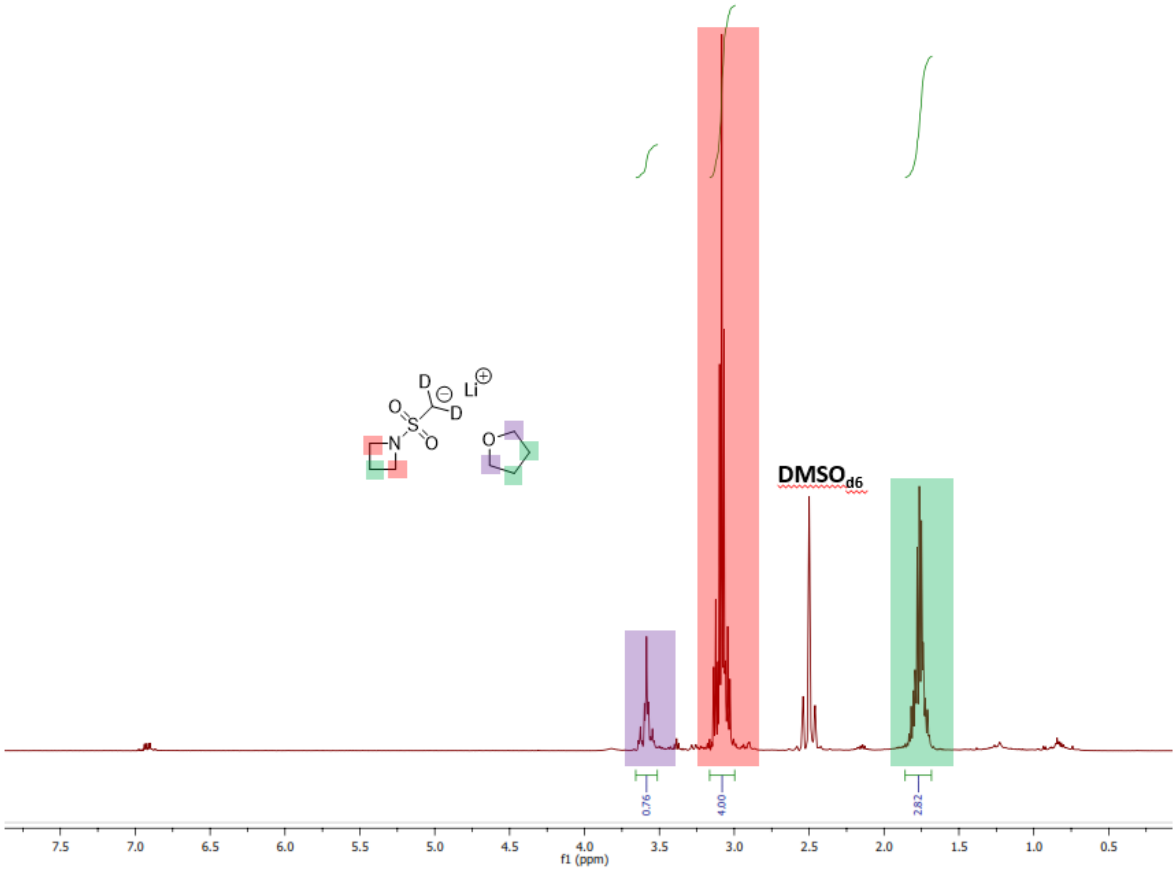

Figure S14. ^{1}H NMR spectrum of **LiMsAzet•THF$_{0.19}$** in DMSO$_{d6}$. The methanesulfonyl group of **LiMsAzet** undergoes H-D exchange in DMSO$_{d6}$ at room temperature. Therefore, signals attributable to the methanesulfonyl protons are not visible.

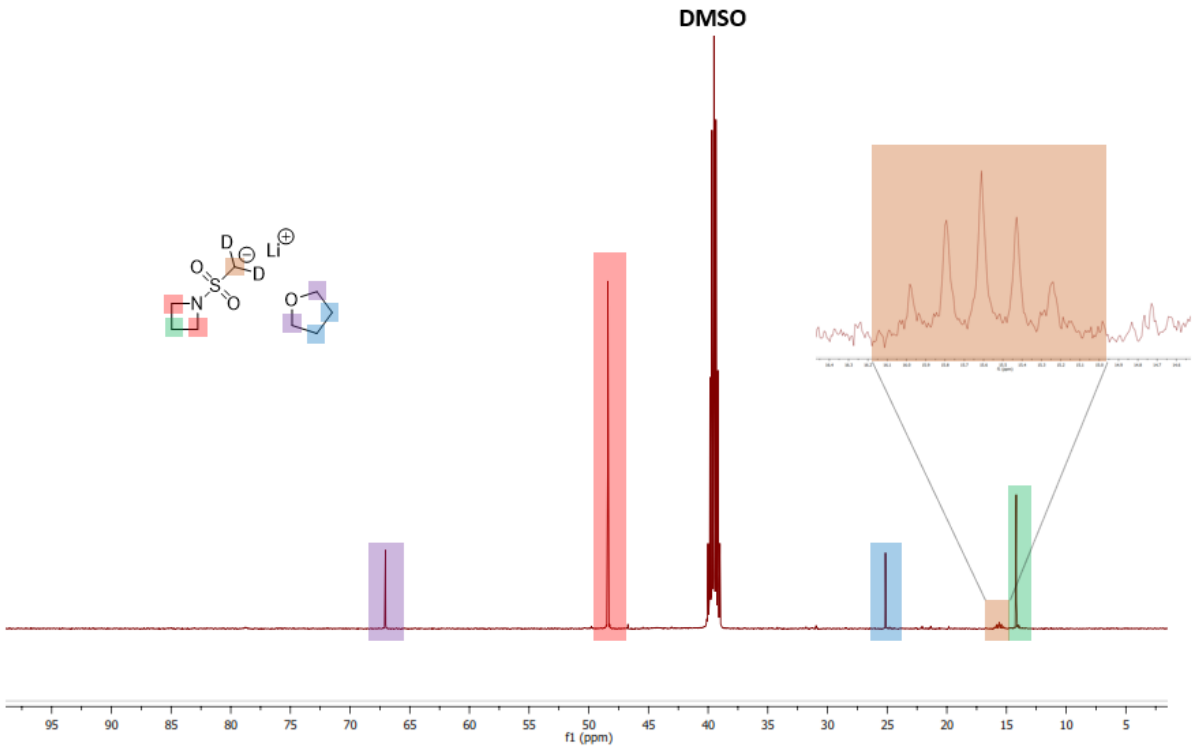

Figure S15. ^{13}C NMR spectrum of **LiMsAzet•THF$_{0.19}$** in $DMSO_{d6}$. The methanesulfonyl group of **LiMsAzet** undergoes H-D exchange in $DMSO_{d6}$ at room temperature. This phenomenon leads to this carbon resonance splitting into a quintet.

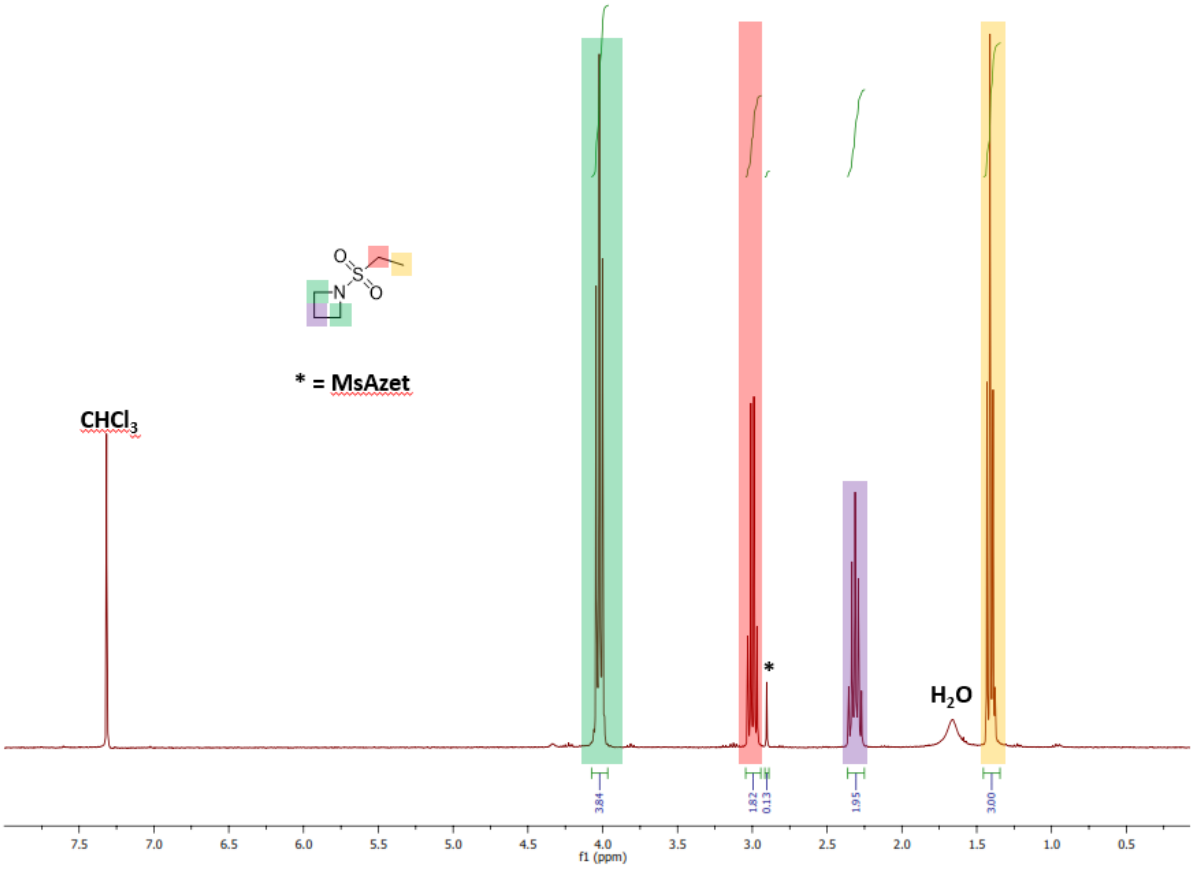

Figure S16. ^{1}H NMR spectrum of *N*-(ethanesulfonyl)azetidine (**EsAzet**) synthesized from **LiMsAzet** in $CDCl_3$. The identity of **EsAzet** was verified by comparison to an authentic sample (see Figure S10). A small amount of **MsAzet** (labeled with *) is also present.

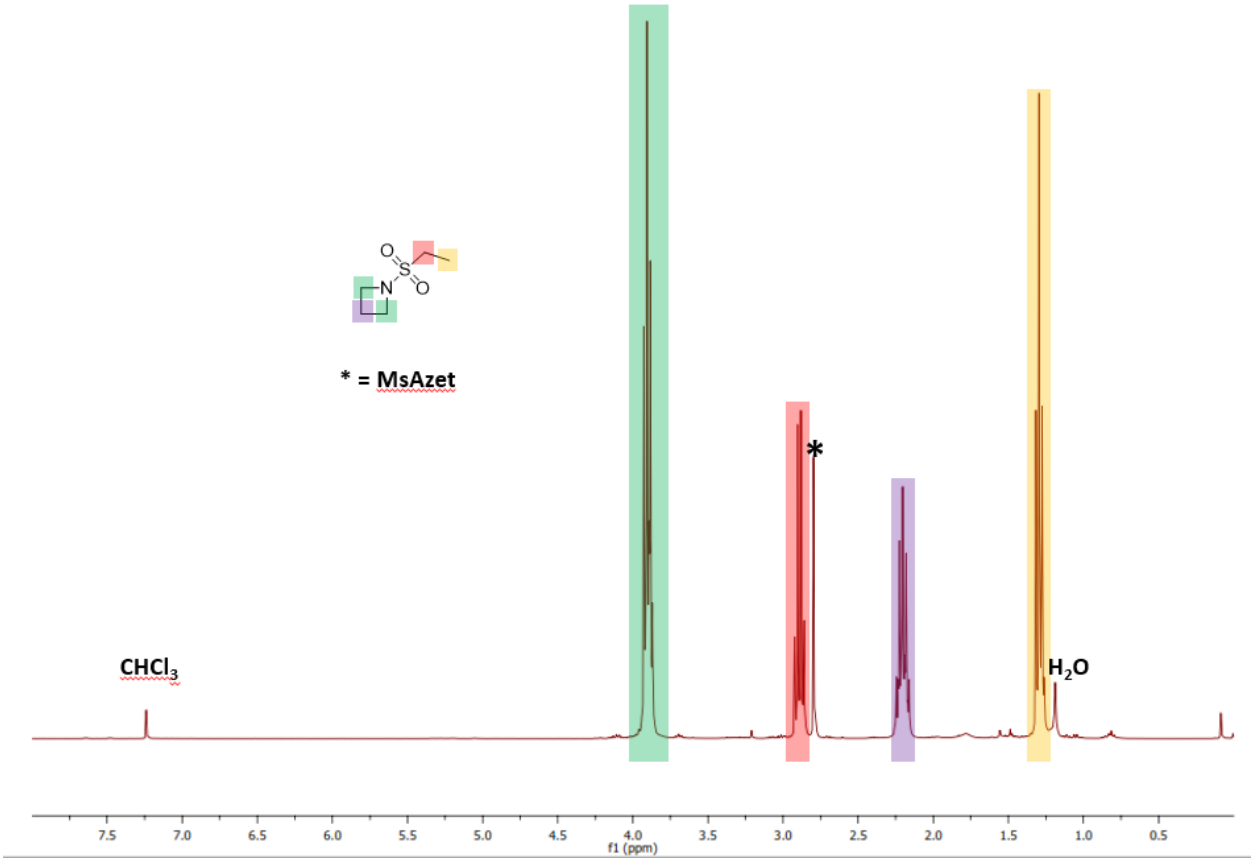

Figure S17. ^{1}H NMR spectrum of *N*-(ethanesulfonyl)azetidine (**EsAzet**) synthesized from **KMsAzet** in $CDCl_3$. The identity of **EsAzet** was verified by comparison to an authentic sample (see Figure S10). A small amount of **MsAzet** (labeled with *) is also present.

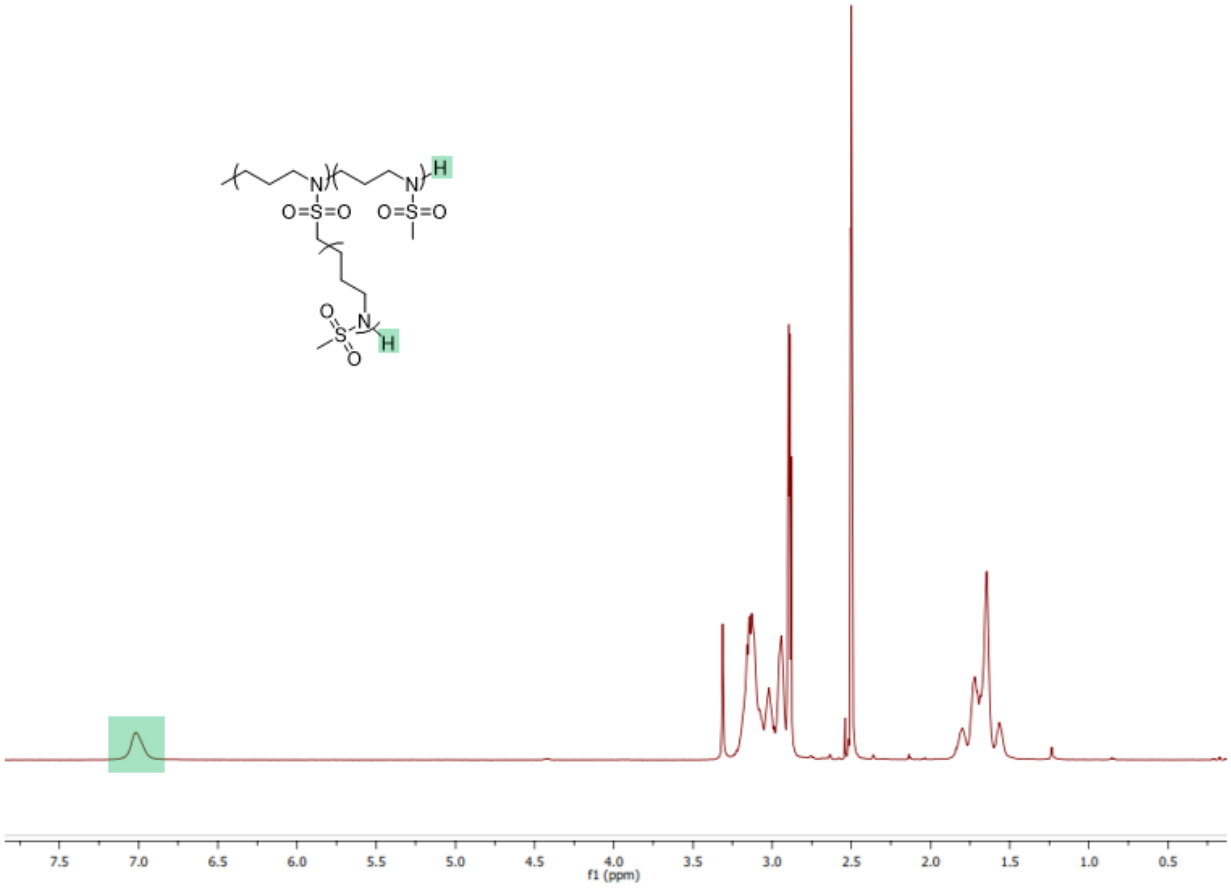

Figure S18. ^{1}H NMR spectrum ($DMSO_{d6}$) of p(MsAzet)^{KMsAzet} initiated by **KMsAzet**. This polymer was synthesized in $DMSO_{h6}$. The spectrum is different than that of p(MsAzet) initiated by ^{n}BuN(K)Ms, likely due to the high degree of branching. See Figs. S23-24 for further support of branching.

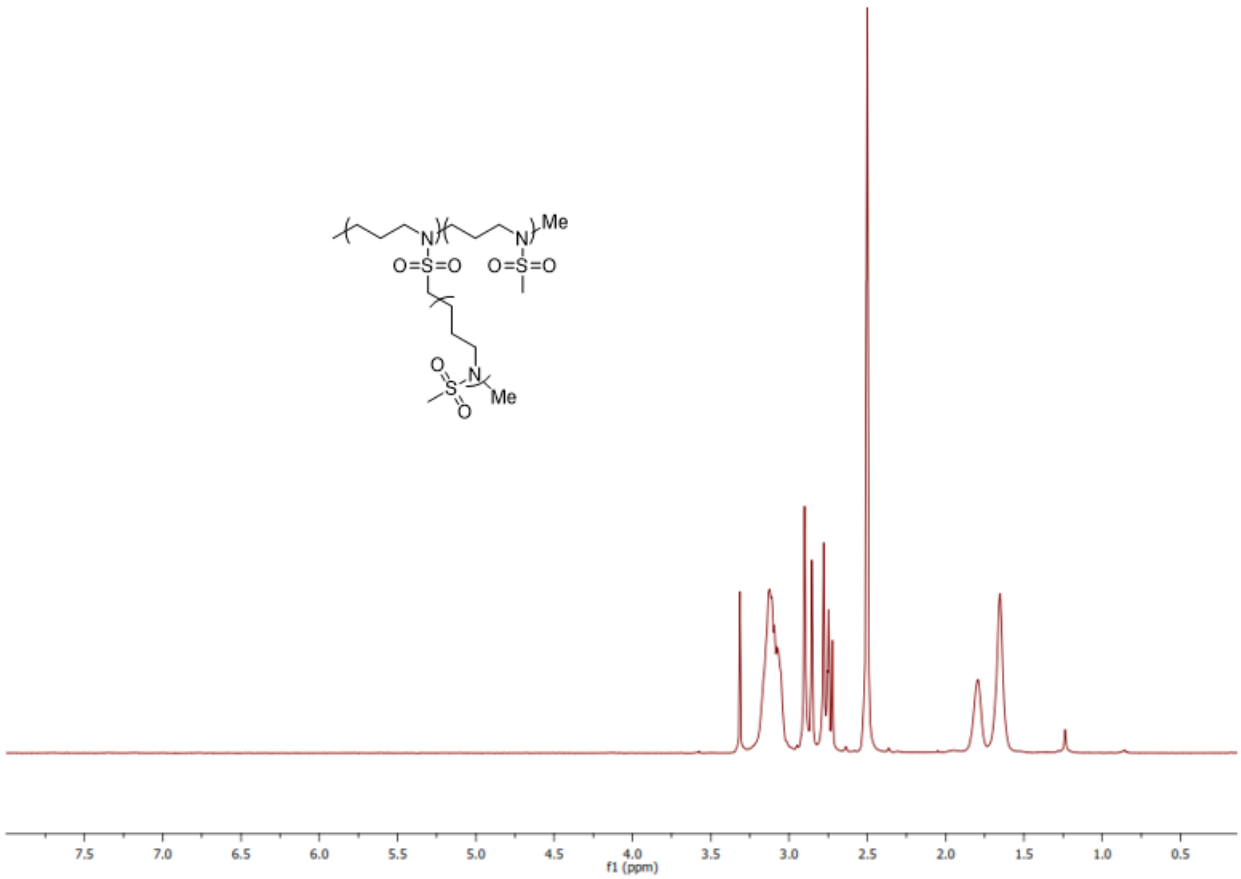

Figure S19. ^{1}H NMR spectrum ($DMSO_{d6}$) of p(MsAzet)^{KMsAzet}, initiated by **KMsAzet**, and subsequently reacted with MeI and Cs_2CO_3, which methylates each N*H* moiety in the polymer. Note the disappearance of the amide proton compared to Figure S18. This polymer was synthesized in $DMSO_{h6}$. See Figs. S23-24 for further support of branching.

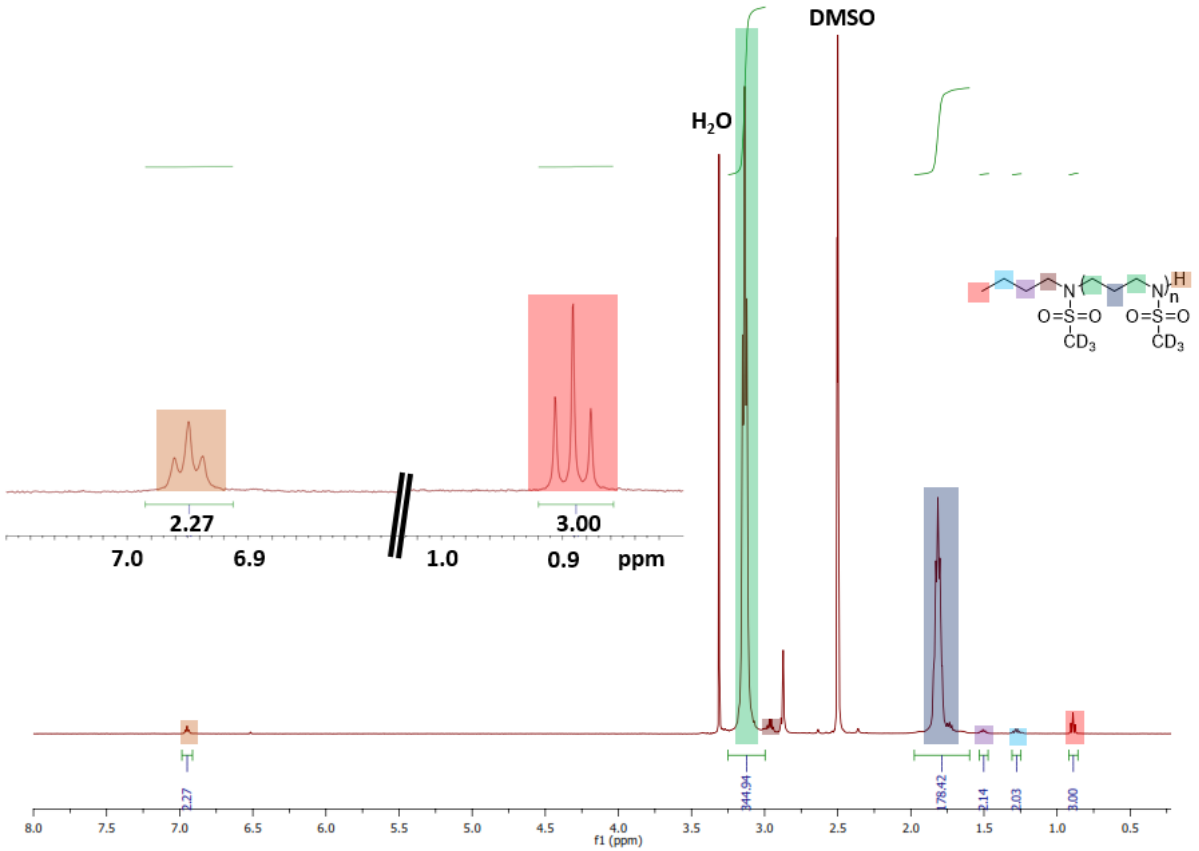

Figure S20. ^{1}H NMR spectrum of deuterated p(MsAzet) in $DMSO_{d6}$ corresponding to Entry 6 in Table 2. This polymer was synthesized in $DMSO_{d6}$. The inset shows the end group integrations indicative of chain transfer. If p(MsAzet) were linear, the expected ratio of the ^{n}BuNMs methyl:MsNH would be 3:1.

MALDI-TOF Mass Spectra

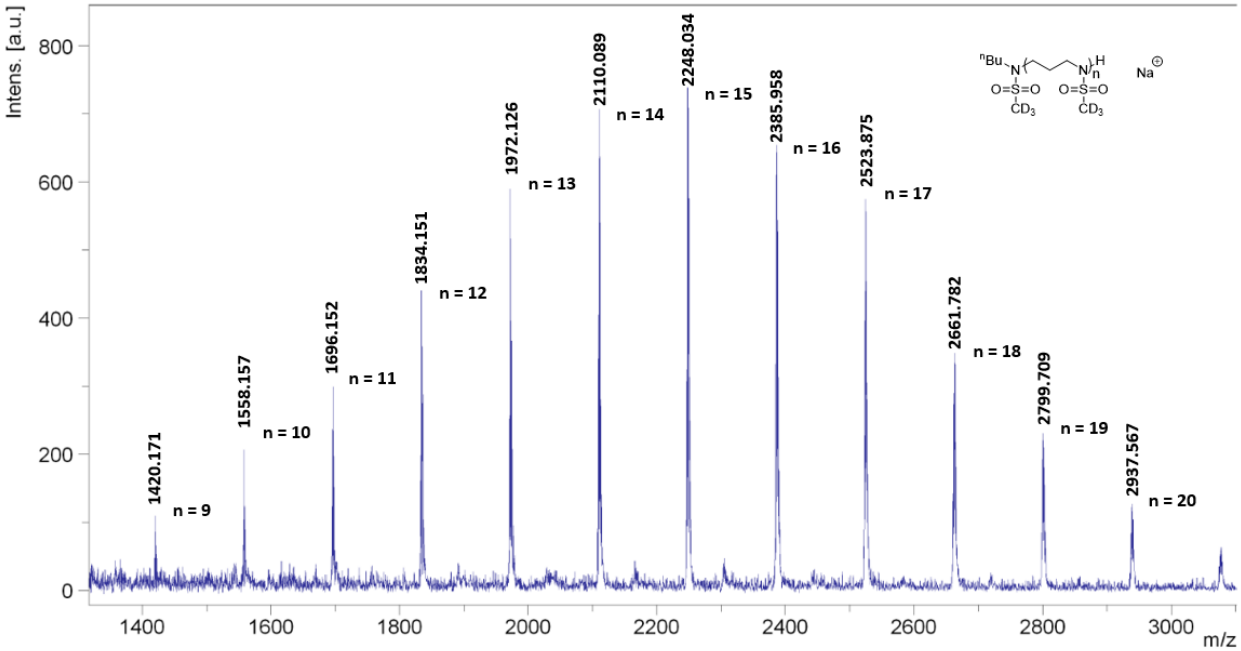

Figure S21. MALDI-TOF MS of p(MsAzet) initiated by ^{n}BuN(K)Ms. This polymerization was performed in $DMSO_{d6}$, which leads to deuteration of the methanesulfonyl groups.

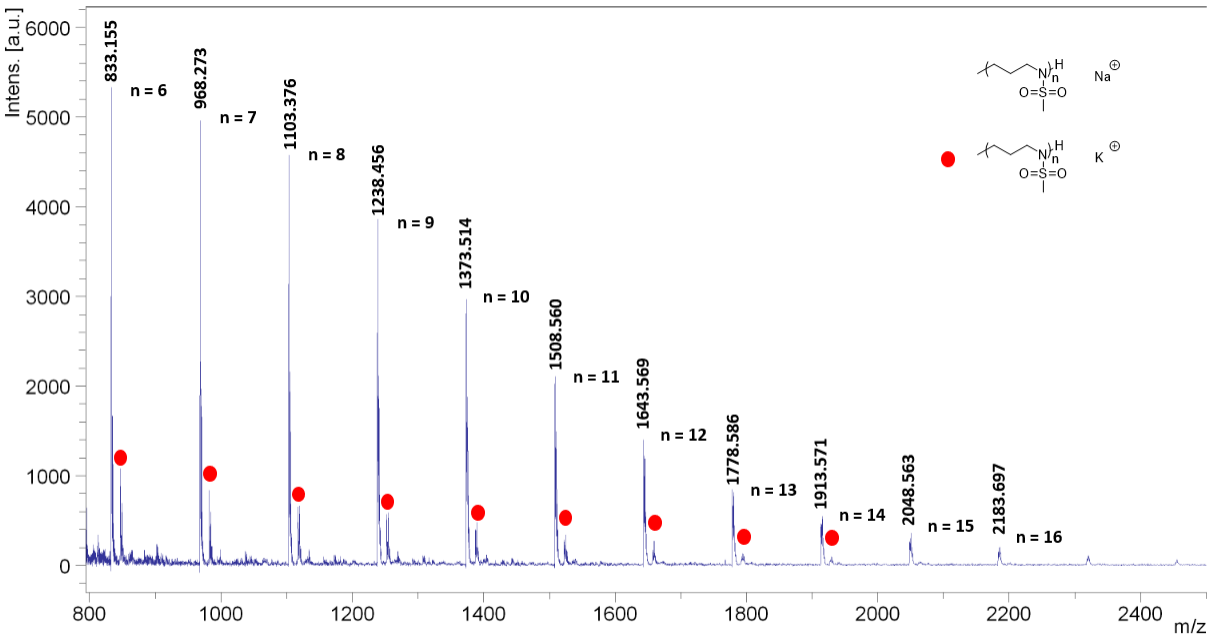

Figure S22. MALDI-TOF MS of p(MsAzet) initiated by **KMsAzet**.

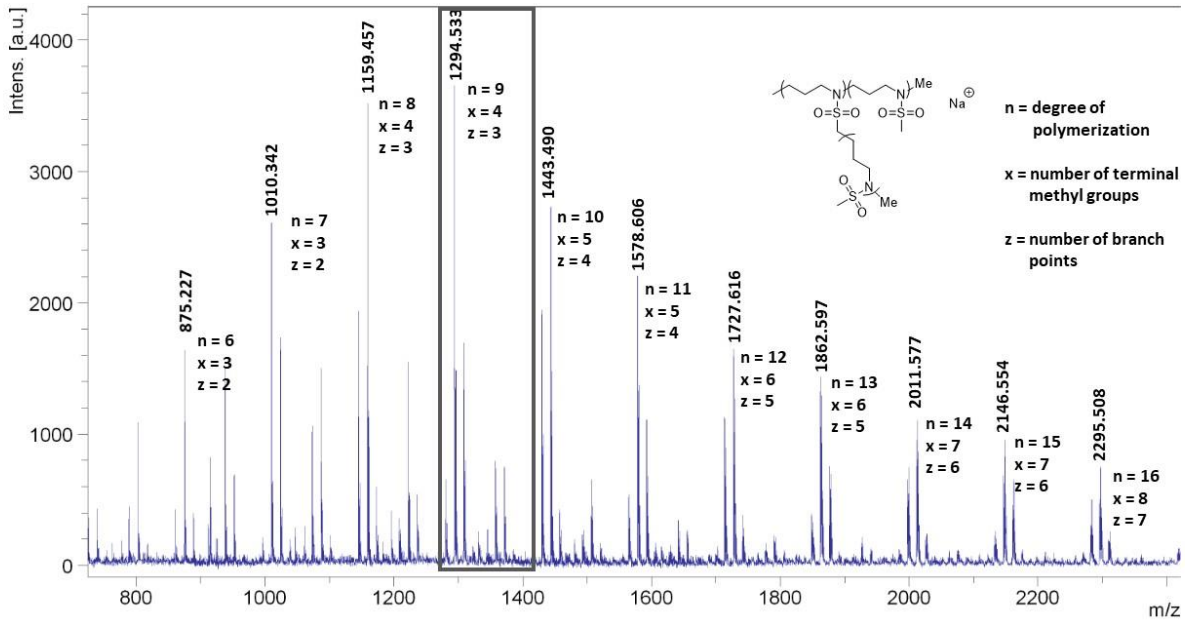

Figure S23. MALDI-TOF MS of p(MsAzet)^{KMsAzet}, initiated by **KMsAzet** and subsequently reacted with MeI and Cs_2CO_3, which methylates each N*H* moiety in the polymer. For further explanation of the lower intensity distributions, see Fig. 3 and S24 for the inset from 1260-1400 m/z. The prominent series in this spectrum is labeled with values of n, x, and z, where n is the number of **MsAzet** repeat units, x is the number of methylated NH moieties, and z = x-1, which is the number of branch points based on the degree of methylation.

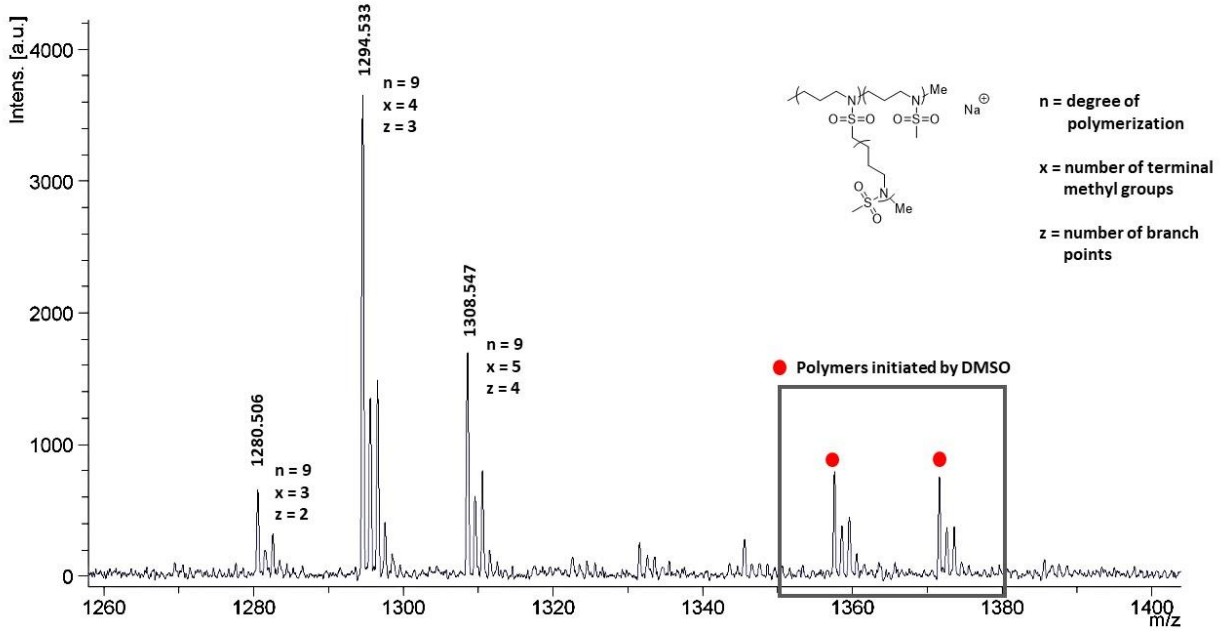

Figure S24. Inset of Fig. S23: MALDI-TOF MS of p(MsAzet)^{KMsAzet}, initiated by **KMsAzet** and subsequently reacted with MeI and Cs_2CO_3, which methylates each N*H* moiety in the polymer. The prominent series in this spectrum is labeled with values of n, x, and z, where n is the number of **MsAzet** repeat units, x is the number of methylated NH moieties, and z = x-1, which is the number of branch points based on the degree of methylation. The region between 1275 m/z and 1320 m/z is expanded in Figure 3. For further explanation of the polymers initiated by DMSO, see S25 for the inset from 1350-1380 m/z.

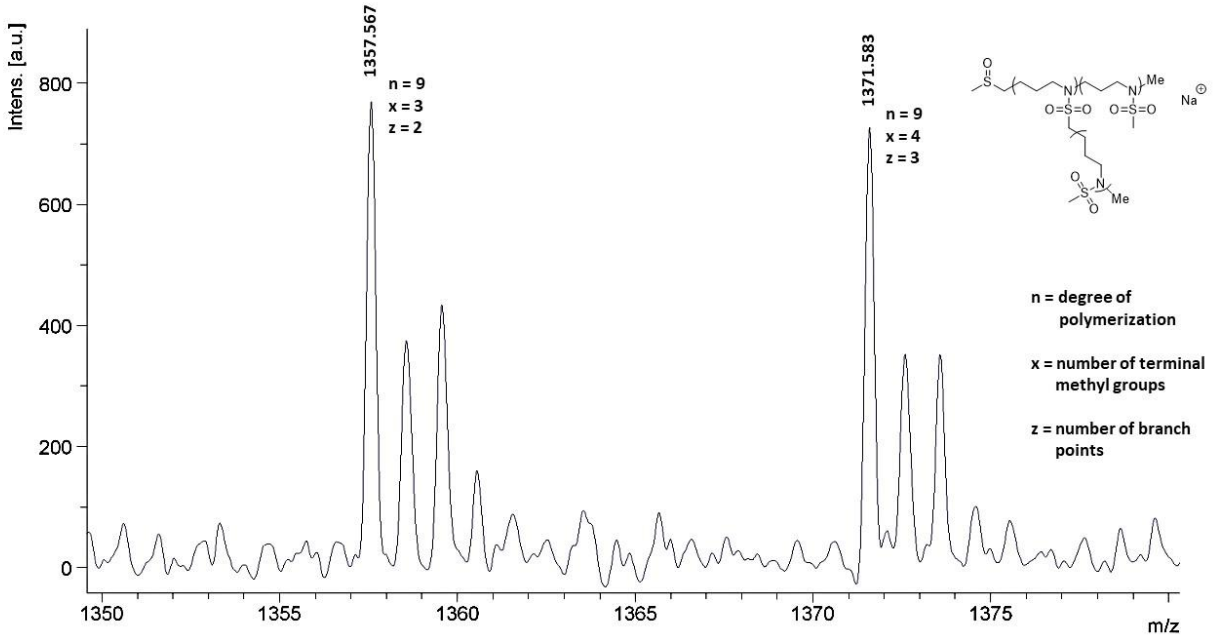

Figure S25. Inset of Fig. S24: MALDI-TOF MS of p(MsAzet)^{KMsAzet}, initiated by **KMsAzet** and subsequently reacted with MeI and Cs_2CO_3, which methylates each N*H* moiety in the polymer. The labeled signals are attributed to polymer chains initiated by the dimsly anion. The prominent series in this spectrum is labeled with values of n, x, and z, where n is the number of **MsAzet** repeat units, x is the number of methylated N*H* moieties, and z = x-1, which is the number of branch points based on the degree of methylation.

SEC

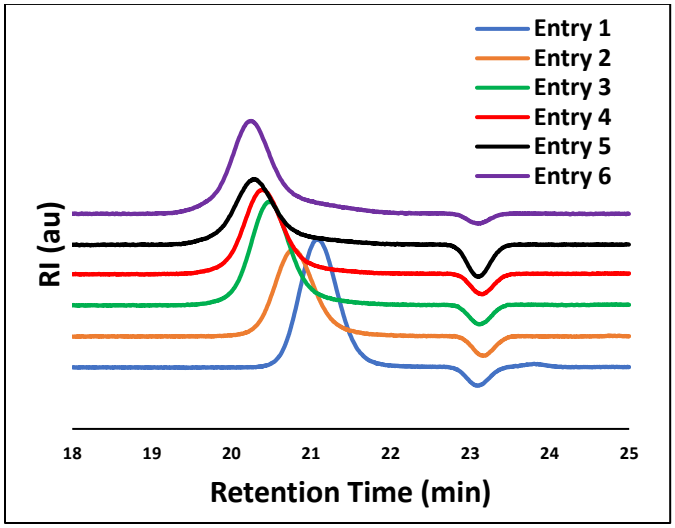

Figure S26. SEC traces of polymers from Table 2.

DSC Analysis

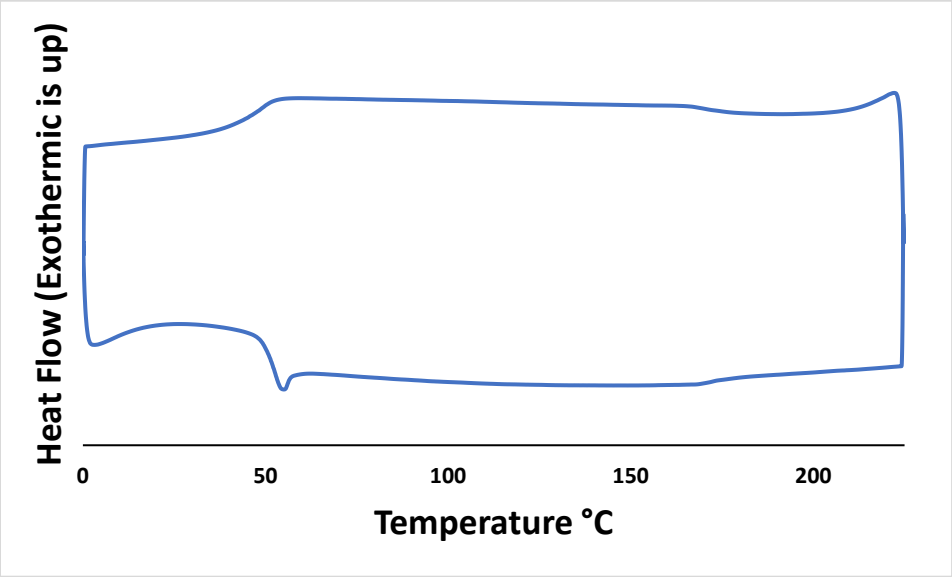

Figure S27. DSC trace of p(MsAzet)$_{50}$ at a heating/cooling rate of 10 °C/min.

TGA Analysis

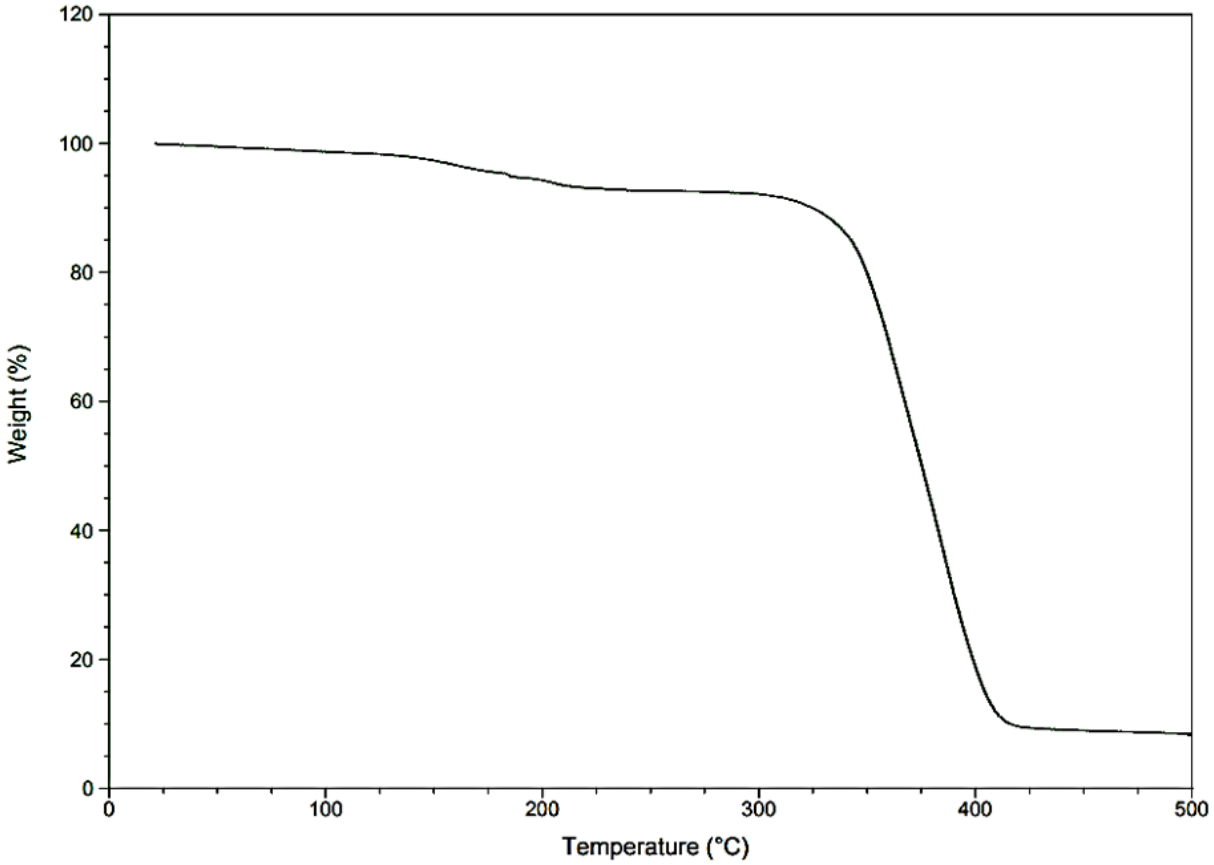

Figure S28. TGA trace of p(MsAzet)$_{50}$ at a heating rate of 10 °C/min.

References

1. Thomi, L.; Wurm, F. R. *Macromol. Symp.* **2015,** *349*, 51-56.
2. Stewart, I. C.; Lee, C. C.; Bergman, R. G.; Toste, F. D. *J. Am. Chem. Soc.* **2005,** *127*, 17616-17617.
3. Reisman, L.; Mbarushimana, C. P.; Cassidy, S. J.; Rupar, P. A. *ACS Macro Lett.* **2016,** *5*, 1137-1140.
4. Gleede, T.; Rieger, E.; Homann-Muller, T.; Wurm, F. R. *Macromol. Chem. Phys.,* **2018,** *219*, 1700145.
5. Homann-Muller, T.; Rieger, E.; Alkan, A.; Wurm, F. R. *Polym. Chem.* **2016,** *7*, 5501-5506.
6. Rieger, E.; Manhart, A.; Wurm, F. R. *ACS Macro Lett.* **2016,** *5*, 195-198.
7. Rieger, E.; Alkan, A.; Manhart, A.; Wagner, M.; Wurm, F. R. *Macromol. Rapid Commun.* **2016,** *37*, 833-839.
8. Rieger, E.; Gleede, T.; Weber, K.; Manhart, A.; Wagner, M.; Wurm, F. R. *Polym. Chem.* **2017,** *8*, 2824-2832.